The $^3F_3$ and the $^1D_2$ Nucleon-Nucleon Partial-Wave Amplitudes in a N/D Model.

R. BHANDARI

Physics Department, New Mexico State University - Las Cruces, NM 88003

(ricevuto l'1 Agosto 1983)

PACS. 13.75. – Hadron-induced low- and intermediate-energy reactions and scattering, energy ≤ 10 GeV.

Summary. – We discuss the energy dependence of the $^3F_3$ and the $^1D_2$ nucleon-nucleon partial-wave amplitudes within the framework of the N/D model, using as input a single pole for the nearby fixed left-hand singularities. Results clearly show dynamical poles as being responsible for the observed structures in the afore-mentioned amplitudes.

The observation of a sharp structure in $\Delta\sigma_L$ (the difference between the proton-proton total cross-sections for parallel and antiparallel longitudinal spin states) in 1977 ([1]) led to the revival of the controversial idea of the existence of dibaryons. The observed presence of structures in the $^3F_3$ and the $^1D_2$ partial-wave amplitudes in the same energy region ($\sim (2.08 \div 2.25)$ GeV centre-of-mass energy) further intensified interest in their possible existence ([2]). Since then, the energy dependence of these amplitudes has been subjected to a great deal of theoretical study ([3-9]) in the hope of resolving the controversy surrounding the dibaryons. This paper is another attempt to understand the prominent structures present in the afore-mentioned amplitudes. The model employed in the study is a N/D model whose main feature is the representation of the nearby left-hand singularities of the partial-wave amplitudes by a single pole.

([1]) For a detailed review of the experimental situation, then, see A. YOKOSAWA: *Phys. Rep.*, **64**, 47 (1980).
([2]) N. HOSHIZAKI: *Prog. Theor. Phys.*, **60**, 1796 (1978); **61**, 129 (1979); R. A. ARNDT: Talk given during *LAMPF Nucleon-Nucleon Workshop, July* (1978).
([3]) B. EDWARDS and G. THOMAS: *Phys. Rev. D*, **22**, 2772 (1980); B. EDWARDS: *Phys. Rev. D*, **23**, 1978 (1981).
([4]) R. BHANDARI, R. A. ARNDT, L. D. ROPER and B. J. VERWEST: *Phys. Rev. Lett.*, **46**, 1111 (1981); R. BHANDARI: *Lett. Nuovo Cimento*, **34**, 65 (1982).
([5]) R. BHANDARI: *Phys. Rev. D*, **27**, 296 (1983).
([6]) R. BHANDARI: *Bull. Am. Phys. Soc.*, **27**, 552 (1982).
([7]) I. DUCK: *Phys. Lett. B*, **106**, 267 (1981).
([8]) W. M. KLOET and J. A. TJON: *Phys. Lett. B*, **106**, 24 (1981); W. M. KLOET and J. A. TJON: Utrecht preprint (1982).
([9]) P. J. MULDERS: *Phys. Rev. D*, **25**, 1269 (1982); E. A. LOMON: *Phys. Rev. D*, **26**, 576 (1982); I. L. GRACH, I. M. NARODETSKY and M. ZH. SHMALIKOV: Preprint ITEP-32 (1983).

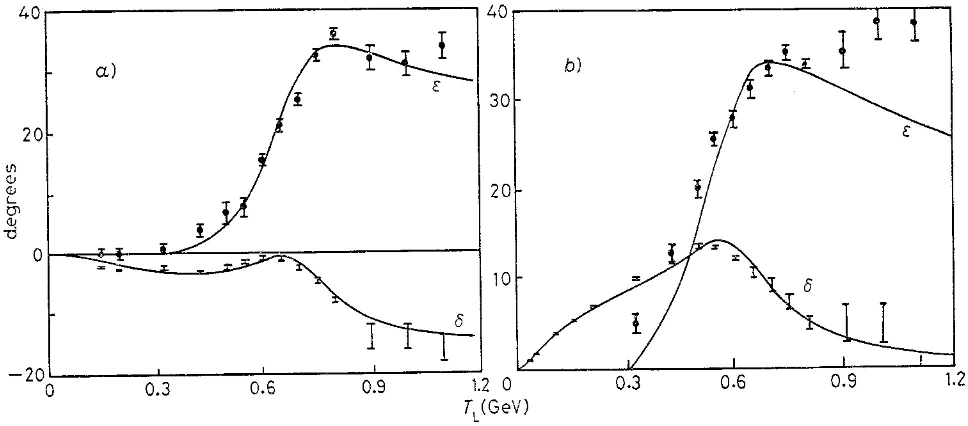

Fig. 1. – *a*) $^3F_3$ and *b*) $^1D_2$ nucleon-nucleon phases δ and ε. The phase ε is related to the conventional elastic parameter η by $\eta = \cos^2\varepsilon$. T_L is the laboratory kinetic energy of the incident nucleon.

Figures 1*a*) and *b*) show the phases for the $^3F_3$ and the $^1D_2$ partial waves, which extend up to a laboratory kinetic energy T_L of 1100 MeV [10]. Since in this energy range the inelasticity is mainly due to pion production and furthermore originates essentially in the $\mathcal{N}\Delta$ channel [11], we consider in our analysis only two channels, $\mathcal{N}\mathcal{N}$ and $\mathcal{N}\Delta$. If we further write the S-matrix as $S(s) = 1 + 2i(\varrho(s))^{\frac{1}{2}}T(s)(\varrho(s))^{\frac{1}{2}}$, where s is the Mandelstam variable, the reduced T-matrix can be expressed as

$$T = ND^{-1}, \tag{1}$$

where N and D are (2×2)-matrices, with N possessing left-hand cuts and D right-hand cuts. It is customary to represent the N-function by a set of poles. In particular, in what follows we use only one pole, *i.e.* we write

$$\operatorname{Im}(N) = -\pi\lambda\delta(s - s_R), \tag{2a}$$

where s_R is real and

$$\lambda = \begin{bmatrix} \lambda_{11} & \lambda_{12} \\ \lambda_{12} & \lambda_{22} \end{bmatrix}, \tag{2b}$$

is a real, symmetric (force-parameter) matrix. The dispersion relations for N and D [12] then imply

$$N_{ij} = \big(\lambda D(s_R)\big)_{ij}/(s - s_R), \tag{3a}$$

$$D_{ij} = \delta_{ij} - \frac{1}{\pi}\big(\lambda D(s_R)\big)_{ij}\int\limits_{s_i}^{\infty}\frac{\varrho_{ii}(s')\,ds'}{(s' - s_R)(s' - s)}, \tag{3b}$$

---

[10] R. A. ARNDT: private communication.
[11] S. MANDELSTAM: *Proc. R. Soc. London, Ser. A*, **244**, 491 (1958); D. V. BUGG: *J. Phys. G*, **5**, 1349 (1977).
[12] See, for example, H. BURKHARDT: *Dispersion Relation Dynamics* (Amsterdam, 1969).

where s_i and ϱ_{ii} denote, respectively, the threshold energy squared and the phase-space factor for the i-th channel. For the channels $\mathcal{N}\mathcal{N}$ and $\mathcal{N}\Delta$ considered in this model, the phase-space factors used are, respectively,

$$\varrho_{11} = \left((s-s_1)/(s-\alpha_1)\right)^{l_e+\frac{1}{2}}, \tag{4a}$$

$$\varrho_{22} = \frac{1}{(s-\alpha_2)^{l_i+\frac{1}{2}}} \int\limits_{M_{\rm T}=M_{\mathcal{N}}+M_\pi}^{\sqrt{s}-M_{\mathcal{N}}} \frac{(s-(M_{\mathcal{N}}+M)^2)^{l_i+\frac{1}{2}}(M-M_{\rm T})^{\frac{3}{2}}\,\mathrm{d}M}{(M+\alpha_0)^{2l_i+2}[(M-M_0)^2+\Gamma^2/4]}, \tag{4b}$$

where the parameters α_1 and α_2 determine the behavior of ϱ_{11} and ϱ_{22} away from their respective thresholds. In addition, they provide distant left-hand singularities to the amplitudes. Similarly, the parameter α_0 controls the behavior in the M-dependence. Such forms of phase-space factors with the correct threshold behavior have been used successfully before ([3-7]). $M_{\mathcal{N}}$ and M_π are the nucleon and the pion masses, respectively. The Breit-Wigner factor in eq. (4b) corresponds to the complex mass $M_\Delta = M_0 - i\Gamma/2 = (1.21 - i0.05)$ GeV. The relative orbital angular momentum l_i in channel $\mathcal{N}\Delta$ is 0 or 1 according to whether the case under consideration is the $^1D_2$ ($l_e=2$) or the $^3F_3$ ($l_e=3$). The elements D_{11} and D_{12} possess the $\mathcal{N}\mathcal{N}$ (nucleon-nucleon) unitarity cut, while the elements D_{21} and D_{22} have, in addition to the $\mathcal{N}\mathcal{N}\pi$ cut (logarithmic in nature), the square-root $\mathcal{N}\Delta$ cuts on the unphysical sheets associated with the $\mathcal{N}\mathcal{N}\pi$ cut. In ref. ([13]), we have given the structure of the D-matrix for the general case. Also given therein are analytic expressions from which the elements D_{11} and D_{12} are calculated, and also the detailed prescription for analytically continuing the elements D_{21} and D_{22} into different sheets in the complex s-plane. The right-hand cut structure of the T-matrix is shown in fig. 2.

The λ-matrix in eq. (2b) is determined by fitting the elastic amplitude $\varrho_{11}T_{11}$, calculated from eqs. (1)-(4), to the phases shown in fig. 1. Table I summarizes the

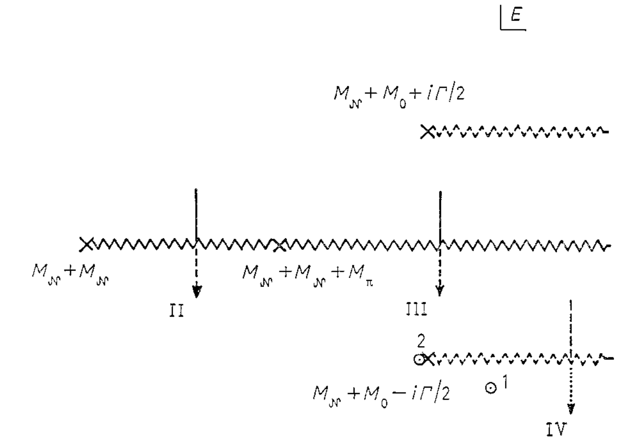

Fig. 2. – Right-hand cut structure of the T-matrix in the complex E-plane where $E=\sqrt{s}$ is the center-of-mass energy. Each arrow leads to a different unphysical sheet. The observed $^3F_3$ and $^1D_2$ poles, marked 1 and 2, respectively, are located on sheet IV. The input pole at $s=s_{\rm R}$ (not shown) is a few MeV below the $\mathcal{N}\mathcal{N}$ branch point on the physical sheet (sheet I) (see table I).

([13]) R. BHANDARI: *Phys. Lett. B*, **121**, 279 (1983).

TABLE I. – *Parameters of the fit and the observed pole's position.* The sheet on which the pole lies is also indicated. See fig. 2 for the labeling of the sheets.

Parameters	$^3F_3$	$^1D_2$
α_1	2.49 (GeV)^2	3.04 (GeV)^2
α_2	2.47 (GeV)^2	2.04 (GeV)^2
α_0	0.06 GeV	-0.94 GeV
$\sqrt{s_1}-\sqrt{s_R}$	5.5 MeV	7.0 MeV
λ_{11}	-1.38 (GeV)^2	0.31 (GeV)^2
λ_{22}	16.2 (GeV)^2	2.97 (GeV)^2
λ_{12}	4.2 (GeV)^2	1.72 (GeV)^2
pole's position	$(2.19-i0.06)$ GeV	$(2.148-i0.049)$ GeV
	(sheet IV)	(sheet IV)

results of the fits also displayed in fig. 1. In the case of the $^3F_3$, the parameter λ_{11} assumes a negative value in order to give negative phase shift to the $^3F_3$ partial-wave amplitude. The large value, 16.2 (GeV)^2, for λ_{22} implies a strong attractive force, in the $\mathcal{N}\Delta$ channel as a result of which a resonance pole at $(2.19-i0.06)$ GeV is observed on sheet IV (see fig. 2). The pole is strongly coupled to the $\mathcal{N}\Delta$ channel. Its effect shows up in the elastic channel through the channel-coupling force parameter λ_{12} ($=4.2$ (GeV)^2); hence the observed dip in the $^3F_3$'s phase-shift δ. It is worthwhile mentioning here that because of the weak coupling to the $\mathcal{N}\mathcal{N}$ channel ($\lambda_{12}=4.2$ (GeV)^2), there is present, in fact, another pole at $\sim(2.2-i0.05)$ GeV. This pole is on a sheet which differs from sheet IV in that $(s-s_1)^{\frac{1}{2}}$ is positive rather than negative on this sheet. When $\lambda_{12}\to 0$, this pole and the pole on sheet IV (which has direct influence on the physical energy region) coincide. Since we will be considering this limit very frequently in our discussions, we shall henceforth ignore the pole at $\sim(2.2-i0.05)$ GeV. Figure 3 shows the Argand plots of the amplitudes

$$\varrho_{11}T_{11}(\mathcal{N}\mathcal{N}\to\mathcal{N}\mathcal{N})\,,\qquad \varrho_{11}^{\frac{1}{2}}T_{12}\varrho_{22}(\mathcal{N}\mathcal{N}\to\mathcal{N}\Delta)\,,\qquad \varrho_{22}P_{22}(\mathcal{N}\Delta\to\mathcal{N}\Delta)\,.$$

The 2.19 GeV center-of-mass energy point (which is the real part of the pole's position) is marked on the trajectories as circles. The upper ends of the trajectories correspond to a center-of-mass energy of 2.3 GeV. The clear counterclockwise looping corroborates the resonant nature of the observed pole. The large loop for the $\mathcal{N}\Delta\to\mathcal{N}\Delta$ amplitude indicates the highly inelastic nature of the pole. Letting $\lambda_{12}\to 0$ (which corresponds to the decoupling of the two channels $\mathcal{N}\mathcal{N}$ and $\mathcal{N}\Delta$) results in the disappearance of the pole in the T_{11} amplitude, confirming its origin in the $\mathcal{N}\Delta$ channel. Furthermore, upon increasing λ_{22}, which corresponds to increasing the attractive interaction in the $\mathcal{N}\Delta$ channel, the pole travels directly towards the $\mathcal{N}\mathcal{N}\pi$ branch point, burrowing through the $\mathcal{N}\Delta$ cut near the $\mathcal{N}\Delta$ branch point on its way and appearing on sheet III (see fig. 2). This is a characteristic feature of such a pole in the N/D formalism, and can be easily understood in the stable-particle limit, *i.e.* in the limit $\Gamma\to 0$, where Γ is the width of the Δ-isobar. In this limit, the three-body $\mathcal{N}\mathcal{N}\pi$ cut disappears and the T-matrix acquires the usual 4-sheet structure with the square-root $\mathcal{N}\Delta$ branch point lying on the real-energy axis. Since the pole originates in the $\mathcal{N}\Delta$ channel and λ_{12} is fairly small relative to λ_{22}, in what follows, we further set λ_{12} equal to zero. This decouples the $\mathcal{N}\mathcal{N}$

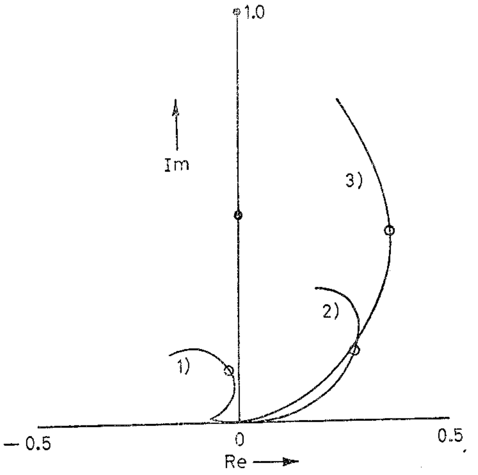

Fig. 3. – Trajectories 1), 2) and 3) are the Argand plots of the amplitudes $\mathcal{N}\mathcal{N} \to \mathcal{N}\mathcal{N}(\varrho_{11}T_{11})$ $\mathcal{N}\mathcal{N} \to \mathcal{N}\Delta(\varrho_{11}^{\frac{1}{2}}T_{12}\varrho_{22}^{\frac{1}{2}})$ and $\mathcal{N}\Delta \to \mathcal{N}\Delta(\varrho_{22}T_{22})$, respectively, for the $^3F_3$ case. Circles correspond to the energy point $E = 2.19$ GeV, while the upper end of each tracjectory corresponds to $E = 2.30$ GeV.

channel from the $\mathcal{N}\Delta$ channel. Figure 4 shows, therefore, only the $\mathcal{N}\Delta$ cut and the positions of the $^3F_3$ and the $^1D_2$ poles obtained in this limit. With increasing values of λ_{22}, the $^3F_3$ pole moves towards the $\mathcal{N}\Delta$ branch point, goes around it from the right and travels to the left along the real-energy axis. On the real-energy axis, the pole is considered a bound-state of the $\mathcal{N}\Delta$ system, in much the same way as a pole below the $\mathcal{N}\mathcal{N}$ threshold in the $^3S_1$ $\mathcal{N}\mathcal{N}$ partial-wave amplitude represents the deuteron. In the limit $\lambda_{22} \to \infty$, the pole coincides with the fixed-input pole at $s = s_R$. It is important to mention here that the complex conjugate counterpart of the $^3F_3$ pole in fig. 4 remains on sheet II and appears on the real-energy axis with increasing values of λ_{22}, while on the real energy axis it is classified as an antibound state of the $\mathcal{N}\Delta$ system. See ref. (12) for further details of this one-channel case discussion.

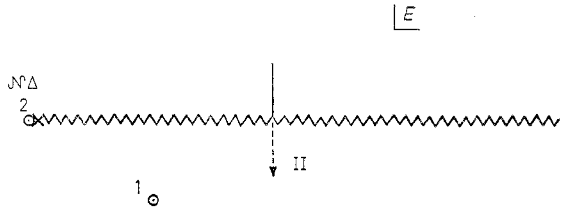

Fig. 4. – The two-sheet cut structure after the $\mathcal{N}\mathcal{N}$ channel is decoupled ($\lambda_{12} = 0$) and the width of the Δ-isobar Γ is reduced to zero. The pole positions are also indicated as 1 and 2 for the $^3F_3$ and the $^1D_2$ cases, respectively.

The observed $^1D_2$ pole by virtue of its position (see fig. 2 and table I) is classified as an antibound state. It also originates in the $\mathcal{N}\Delta$ channel. When λ_{22} is increased, the pole goes round the $\mathcal{N}\Delta$ branch point to appear on sheet III and moves to the left thereafter. When lying to the left of the $\mathcal{N}\Delta$ branch point in sheet III it is considered a bound state of $\mathcal{N}\Delta$ system. These features of the $^1D_2$ pole reminiscent of the behavior of the dynamical pole in the one-channel case corresponding to $l_i = 0$ (s-wave) are verified in the limit $\Gamma \to 0$ and $\lambda_{12} \to 0$. In this limit, the observed $^1D_2$ pole lies on the real-energy axis below the $\mathcal{N}\Delta$ branch point as shown in fig. 4 (see also ref. (12)).

The afore-mentioned discussion regarding the nature of the poles was reduced to one within the framework of the one-channel stable-particle case in the limits $\Gamma \to 0$ and $\lambda_{12} \to 0$. Consideration of the latter limit was justified on the grounds that the origin of the poles in each of the two partial-wave amplitudes was in the $\mathcal{N}\Delta$ channel and λ_{12} was small compared to λ_{22}. Furthermore, in this limit, there were 2 dynamical poles in the case of $^3F_3$ ($l_i = 1$) and one dynamical pole (on the real-energy axis) in the case of $^1D_2$ ($l_i = 0$). In fact, a careful study of the analytic expressions for the D-function given in ref. (13) reveals that, for a partial-wave amplitude corresponding to orbital angular momentum l_i, there are $l_i + 1$ dynamical poles in the vicinity of the threshold. One of these always originates from $s = s_R$ on the unphysical sheet. Furthermore, when l_i is even as in the $^1D_2$ case ($l_i = 0$), it always remains on the real-energy axis and changes from the antibound-state type to the bound-state type with increasing values of the force-parameter λ.

In conclusion, if the nearby left-hand singularities of the T-matrix for $\mathcal{N}\mathcal{N}$ and $\mathcal{N}\Delta$ channels can be represented by a single pole (below the $\mathcal{N}\mathcal{N}$ threshold) in the N-matrix, calculations within the framework of the N/D formalism indicate that the structures in the $^3F_3$ and the $^1D_2$ partial-wave amplitudes are due to nearby dynamical poles which are highly inelastic. While the pole in the case of the $^3F_3$ amplitude is of the conventional resonance type consistent with the previous analyses (3-8), the results for the $^1D_2$ partial-wave amplitude show the pole to be of the antibound type, lying very close to the $\mathcal{N}\Delta$ branch point. This close proximity of the $^1D_2$ pole to the $\mathcal{N}\Delta$ branch point has been observed earlier also (3,5,6,8). However, its interpretation, for example, in ref. (5) was different, *i.e.* it was described therein as a channel-coupling pole. Furthermore, the author of ref. (7), employing the N/D formalism with a large number of input poles, found no dynamical pole in the $^1D_2$ partial-wave amplitude. The conflicting results regarding the $^1D_2$ partial-wave amplitude suggest the need for a more thorough examination of this amplitude, which was also pointed out in (5).